Macromolecules

Surface Charged Polymeric Micelles—A Tunable Model System Studied by SANS

Lingsam Tea, Luis Willner, Christin Waldorf, Olga Matsarskaia, Ralf Schweins, Stephan Förster, Lutz Willner,* and Jörg Stellbrink*



Cite This: Macromolecules 2024, 57, 5818-5830



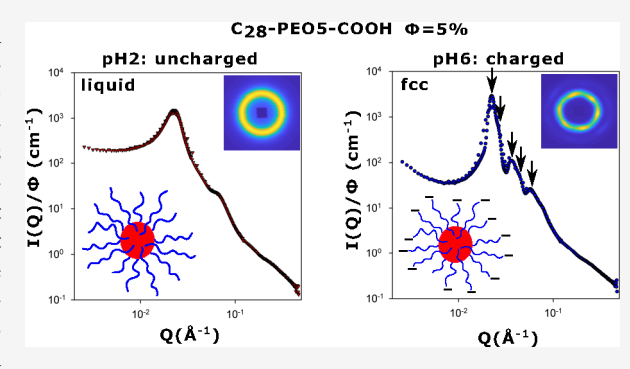
ACCESS I

Metrics & More

Article Recommendations

Supporting Information

ABSTRACT: We investigate surface charged "starlike" micelles in aqueous solution formed by carboxy terminated n-octacosyl-poly-(ethylene oxide) block copolymers, C₂₈-PEO5-COOH with 5 the PEO molar mass in kg/mol, by small angle neutron scattering (SANS), zetapotential measurements, and rheology. The -COOH end group was introduced by selective oxidation of the -CH₂-OH end group of a C₂₈-PEO5-OH precursor using Bobbitt's salt. Micellar solutions of different concentrations in the dilute and semidilute range were investigated at pH 2, 6, and 12 to vary ionic strength and the number of effective surface charges $Z_{\rm eff}$, $Z_{\rm eff}$ was further varied by using mixtures of C_{28} -PEO5-COOH and C28-PEO5-OH at different mixing ratios. SANS measurements reveal that the intramicellar form factor P(Q) is identical



at the different pH values, which implies that the individual micellar structure is unaffected by the number of surface charges. On the contrary, the intermicellar structure factor S(Q) and the phase behavior show a strong dependence on Z_{eff} . In particular, we observe a distinct shift of the liquid-fcc crystal phase boundary. A quantitative analysis in terms of a screened Hard Sphere Yukawa potential reveals very good agreement between experiment and theory. Because of this consistency and of the tunability of the n-alkyl-PEO starlike micelles, we consider this system to be an excellent model for further studies on the interplay between steric and electrostatic interactions in soft colloids.

INTRODUCTION

Sterically stabilized colloids constitute an important class of soft matter materials encompassing regular star polymers, polymer micelles, microgels, and polymer grafted nanoparticles. The term "softness" can be classified into intra- and interparticle softness.^{1,2} Intraparticle softness refers to the deformability and compressibility of an individual particle, whereas interparticle softness is linked to particle interactions described by an effective pair potential. An ultrasoft potential to describe repulsive interactions of regular star polymers was derived by Likos et al.³ This potential combines a logarithmic form at small interparticle distances and screened Yukawa-type exponential behavior at larger distances. The number of arms is the only control parameter for star-star interactions varying from 2 for a linear polymer chain to ∞ for hard spheres. A suitable model system to investigate soft colloidal properties is amphiphilic block copolymer micelles. The number of arms or aggregation number, and thus, their softness can be effectively adjusted by changing block copolymer characteristics⁴⁻⁷ and/ or solvent quality.8

This inherent variability enables systematic studies of interactions and phase diagrams of ultrasoft colloids as already presented in earlier publications. $^{9-11}$ In addition to steric interactions, electrostatic interactions play an important role

for the stabilization of colloidal dispersions. Charge-stabilized dispersions are relevant for many natural and industrial products, such as for food articles, paints, ink, and rubber. A large variety of charged soft colloids have been prepared and investigated by experiments, theory, and computer simulation. Important classes of charged soft colloids are PSS and PMMA latex particles, 12-14 ionic dendrimers, 15-20 polyelectrolyte block copolymer micelles, 21-25 star branched polyelectrolytes^{26–29} and μ -gels.³⁰ The internal particle structure was frequently investigated in dependence of the charge and ionic strength. Moreover, numerous studies were devoted to interparticle interaction. The electrostatic interaction of charged spheres is generally described by a screened Coulomb or Yukawa potential,31 where the main parameters are the (effective) particle charge Z_{eff} the Debye-Hückel screening length κ^{-1} , the particle radius R, and the interparticle distance

Received: February 29, 2024 May 7, 2024 Revised: Accepted: May 23, 2024 Published: June 5, 2024





In the present work, we investigate starlike block copolymer micelles formed by carboxy-terminated n-octacosyl-poly-(ethylene oxide) block copolymers, C28-PEO5-COOH, synthesized by selective end-group oxidation of an anionically polymerized C₂₈-PEO5-OH precursor. Digit 5 denotes the PEO molar mass in kg/mol. Structural properties of micelles formed by the OH-terminated block copolymer have been thoroughly studied and published earlier. 32-36 Since carboxylic acids are weak acids, the number of surface charges can be conveniently varied by adjusting the pH. Thus, we are able to systematically investigate properties of sterically and electrostatically stabilized soft colloids. We particularly emphasize that micellar solutions of C₂₈-PEO5 exhibit fast unimer exchange dynamics as one important prerequisite to reach thermally equilibrated samples after altering experimental parameters, 34,37 even though it has been reported that slower fusion and fission events play an important role to reach equilibrium structures.³⁸ The above-mentioned properties make the C₂₈-PEO5-COOH micelles a "tunable" soft colloidal model which can be classified as hybrid between neutral and polyelectrolyte block copolymer and ionic and nonionic surfactant micelles. Because of the long PEO chain ($N_{PEO} = 113$), it differs from low molar mass polyoxyethylene alkyl ether carboxylic acid surfactants recently studied by Chiappisi et al. ^{39–42} Our study also differs from pH-dependent structural investigations on polyelectrolyte block copolymer micelles, ^{22,23,25} where ionizable groups are located all along the corona blocks. Here, we systematically investigate the intra- and intermolecular structure of surface charged C28-PEO5-COOH micelles as a function of pH, ionic strength, and concentration. We point out that the C₂₈-PEO5-COOH micelles carry only one charge per corona chain in the terminal position. As a main experimental tool we employ small angle neutron scattering (SANS) for the structural study. Micellar interactions are analyzed in terms of the well-established screened Hard Sphere Yukawa potential. In detail, we apply the modified penetrating background rescaled mean spherical approximation (MPB-RMSA), a recent approach introduced and thoroughly discussed by Heinen et al.³¹ Therein, the authors modified/ combined the screened Coulomb repulsion from the Derjaguin-Landau-Verwey-Overbeck (DLVO) potential⁴³ and the RMSA closure⁴⁴ by the penetrating microion background scheme of Snook and Hayter. 45 We obtain very good agreement between experimental and theoretical S(Q) at finite concentrations in the liquid regime. Complementary, the zeta-potential is determined via measurements of the electrophoretic mobility. Liquid-solid transitions are additionally studied by rheology.

EXPERIMENTAL SECTION

Synthesis and Characterization. The carboxy-terminated polymer C_{28} -PEO5-COOH was prepared by oxidation of C_{28} -PEO5-OH using 4-(acetylamino)-2,2,6,6-tetramethyl-1-oxo-piperidinium tetrafluoroborate (Bobbitt's salt) as oxidizing agent. The OH-precursor polymer with a PEO molar mass of 5 kg/mol was synthesized by ring opening living anionic polymerization of ethylene oxide in toluene at 95 °C as described in detail in previous publications. For the -CH₂-OH end-group oxidation, 5 g (~1 mmol) of C_{28} -PEO5-OH was dissolved in 100 mL Milli-Q water until a homogeneous clear micellar solution was obtained. An excess amount of Bobbitt's salt (2.25 g = 7.49 mmol) was added, and the resulting orange solution was stirred for 20 hours at room temperature. Subsequently, 20 mL of sodium bisulfite (40%) and 20 mL of sodium hydroxide solution (20%) were added and stirred for another

hour before the pH was adjusted to ${\sim}3$ with hydrochloric acid. The resulting mixture was then carefully washed five times with 50 mL ethyl acetate to remove residues of Bobbitt's salt. The carboxylated polymer was extracted from the aqueous phase with chloroform ((3–4) \times 50 mL). The combined phases were dried with magnesium sulfate. After filtration, CHCl $_3$ was removed on a rotating evaporator, and the residual polymer was recrystallized three times from acetone at $-20\,^{\circ}\mathrm{C}$.

For further utilization, the polymer was additionally purified by dialysis against ultrapure $\rm H_2O$ (0.055 mS/cm) using Slide-A-Lyzer Dialysis Cassettes G2 with 2.5 kg/mol molar mass cut off from Thermo Fisher Scientific. Polymer solutions in $\rm H_2O$ of $\sim\!3\%$ polymer volume fraction were prepared and dialyzed for at least 72 h. In between, the water bath was exchanged several times until a constant conductivity of about 0.3 - 0.4 mS/cm was obtained. Finally, the polymer was retrieved by freeze-drying the dialyzed polymer solution in vacuum.

The molar characteristics of the C_{28} -PEO5-COOH and -OH polymers were determined by 1 H NMR and size exclusion chromatography (SEC). SEC data were obtained by a chromatographic setup consisting of autosampler, isocratic pump (Agilent Technologies, Series 1260 infinity), column oven (Shimadzu CTO-20A), refractive index detector, 18 angle light scattering detector (Wyatt Technologies, Optilab T-rEX and DAWN HELEOS-II) and three Agilent PlusPore GPC columns with a continuous pore size distribution. A mixture of tetrahydrofuran, N,N-dimethylacetamide, and acetic acid (84:15:1) was taken as eluent. Acetic acid was added in order to prevent interactions of -COOH end-groups with the column material. The measurements were conducted at 40 $^{\circ}$ C at a flux rate of 1 mL/min. Analysis of the SEC data using Astra Software of Wyatt Technologies yields the number and weight-average molar masses, M_n and M_w , and the dispersity M_w/M_n .

 1 H NMR spectra were recorded in pyridine-d5 with a Bruker Avance III 600 MHz spectrometer equipped with a CryoProbe Prodigy. The degree of PEO-polymerization, $N_{\rm PEO}=113$, was determined using the integral intensity of the 57 protons of the n-alkyl resonances as internal reference, and the total number-average molar mass $M_{\rm n}$ calculated thereof. Molar masses and dispersities of the polymers are summarized in Table 1. The 1 H NMR spectra

Table 1. Total Molar Masses^a and Dispersity of the C₂₈-PEO5 Polymer Obtained from NMR and SEC

C ₂₈ -PEO5 5390 5760 5900	1.03					
$^aM_{\rm n/w}=M_{\rm n/w}({\rm PEO})+M({\rm C_{28}H_{57}}=393{\rm g/mol}).$ $^b{\rm From~NMR.~}^c{\rm From~SEC.}$						

additionally served as proof of the completeness of the oxidation process. In pyridine-d5 the signals of the terminal EO units are well separated from the main PEO resonance. These signals show a characteristic change by the oxidation as indicated in the NMR spectra of -OH-terminated and -COOH-terminated polymers shown Figure 1.

Complementary to NMR, the oxidized polymers were reinvestigated by SEC. The elution curves of -OH and -COOH polymers were compared and found to be exactly identical which confirms that no oxidation and/or degradation of the PEO chains occurred. Chromatograms are shown in Figure 2a).

For further characterization, aqueous solutions of the oxidized polymer were titrated with 0.1 M NaOH-solution. pH-values were measured with a Knick Portamess 911 pH-meter combined with a Hamilton BioTrade electrode. The device has been calibrated with Mettler Toledo buffer solutions of pH 4.01, 7, and 9.21. Titration curves for various concentrations are depicted in Figure 2b). Sigmoidal fits were used to extract the equivalence point, which was found at pH 7.9 ± 0.1 for the different concentrations. Moreover, from the initial pH value of each solution, we calculated p K_a -values of 4.3 ± 0.2 , which is a typical value for weak acids.

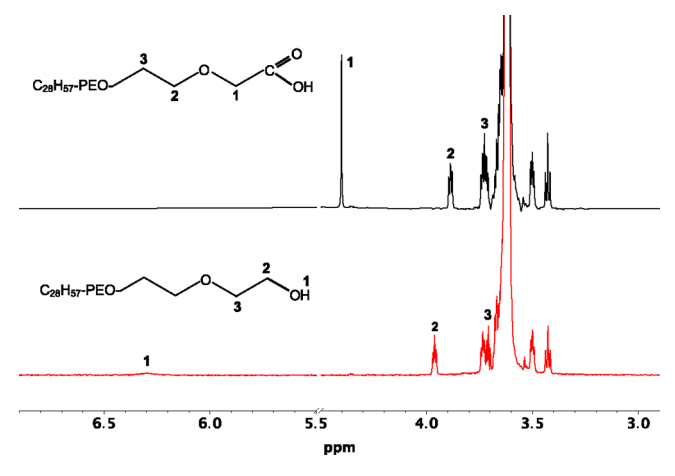


Figure 1. Relevant sections of 1 H NMR spectra of C_{28} -PEO5-OH and -COOH polymers recorded in pyridine-d5. A characteristic shift of signals resulting from the terminal methylene protons is observed after oxidation. Full oxidation can be assumed based on the complete disappearance of signal 2 in C_{28} -PEO5-OH originating from protons adjacent to the hydroxy group.

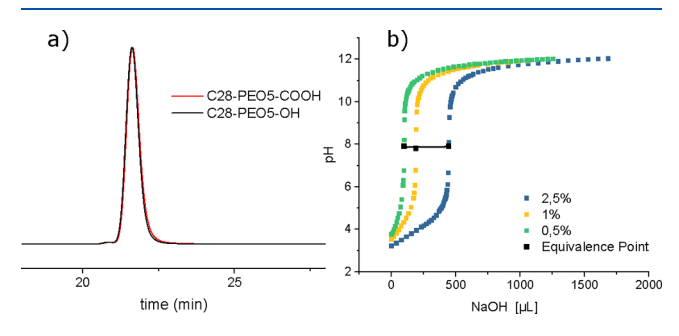


Figure 2. a) SEC-traces of C_{28} -PEO5 polymers before and after endgroup oxidation. b) Titration curves of C_{28} -PEO5-COOH at three different polymer concentrations. Numbers denote nominal polymer volume fraction in %.

Generally, the degree of dissociation α is defined as the concentration of the dissociated form c_{R-COO^-} relative to the total concentration $c_0=c_{R-COO^-}+c_{R-COOH}$, i.e. $\alpha=c_{R-COO^-}/c_0$. It is important to note that for weak acids, α depends on c_0 , which in turn affects the number of charges per micelle. Since $c_{R-COO^-}=c_{H_3O^+}$, the oxonium-ion concentration, the degree of dissociation α of C_{28} -PEO5-COOH solutions were calculated from pH measurements. Accordingly, α varies from 0.04 for polymer volume fraction $\phi=4.7\%$ up to $\alpha=0.46$ for $\phi=0.08\%$. In order to facilitate interpretation of a concentration-dependent study of micellar solutions, a constant number of surface charges per micelles, i.e. $\alpha=$ constant, is desirable. This was achieved by adjusting the pH to 2, 6, and 12 with hydrochloric acid and sodium hydroxide solution. This fixes α to either 0 at pH 2 or 1 at pH 6 and 12, respectively, as described in more detail in the subsequent section.

For SANS experiments, micellar solutions of C_{28} -PEO5-COOH in D_2O (99.9% D) with volume fractions ranging from $\phi=0.05\%$ - 10% were prepared at 3 different pH-values around 2, 6, and 12. pH 2 is reached by addition of more than one equivalent of DCl with respect to the terminal carboxy-groups. At this point, the carboxy groups are essentially undissociated. pH 6 is reached by the addition of almost one equivalent of NaOD. Under these conditions more than 99% of the carboxy groups are dissociated. pH 12 requires more than one equivalent of NaOD, leading to fully dissociated -COOH groups. The difference between the degree of dissociation at pH 6 and pH 12 is small, but the ionic strength [I] is significantly different, \approx 0.7 mmol/L compared to \approx 7 mmol/L, due to the excess amount of sodium and hydroxy ions which screens electrostatic interactions

between micelles (Figure 3). The resulting Debye–Hückel screening length κ^{-1} decreases by a factor of \approx 2. As a reference for uncharged

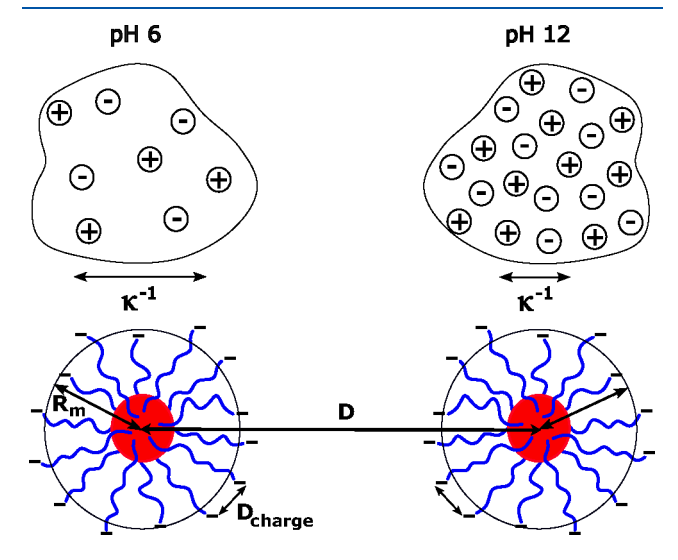


Figure 3. Illustration of characteristic length scales.

micelles, two solutions of C_{28} -PEO5-OH in D_2O at $\phi=0.15\%$ and $\phi=5\%$ were additionally prepared. In order to further vary the number of surface charges, three mixtures of -OH and -COOH terminated polymers at ratios of 3:1, 1:1 and 1:3 have been prepared at $\phi=5\%$ and pH 6. For ζ -potential and viscosity measurements, micellar solutions at $\phi=1\%$ were produced at five different pH-values. For the sake of consistency, these solutions were also prepared in D_2O .

For the preparation of solutions at $\phi = 1$, 4, 5, 7.5 and 10% dry polymer powder were directly solubilized in D2O. In order to support dissolution and ensure micelle equilibration, the polymer/D2O mixtures were initially heated up to 50 °C for 4 h and were subsequently left to cool down to room temperature overnight under constant shaking. For low volume fractions, this procedure leads to homogeneous, clear micellar solutions. At higher concentrations, homogenization was achieved by repeated centrifugation and turning sample vials in between. Solutions with volume fractions $\phi = 0.15\%$ and 2.5% were obtained by dilution of stock solutions of $\phi = 1\%$ and 5%, respectively. Each solution was split into three parts and adjusted to the respective pH by the addition of NaOD (0.185 mol/L) or DCl (0.1 mol/L). After addition, the equilibration procedure, heating for 4 h at 50 °C and shaking overnight at room temperature, was repeated. For some samples at higher concentrations, solidification was observed after the addition of NaOD. In these cases, homogenization was achieved by centrifugation as described above. For the preparation of mixed micelles, 5% stock solutions were mixed at the desired ratio and equilibrated at 50 °C for 4 h. At this temperature, molecular exchange is fast such that a random distribution of -OH and -COOH terminated polymers is guaranteed. 34,37 The mixed micelles were subsequently adjusted to pH 6 with NaOD and again equilibrated by heating to 50 °C for 4 h. The ionic strength [I] of each sample was calculated solely from the amount of excess NaOD or DCl and finally corrected for CO2 absorption at the given experimental pH (see Appendix). We note that an exact adjustment of the pH-values was difficult, in particular at pH 6, because of solidification, limited sample volume, and the required tiny amount of DCl or NaOD. However, all important parameters were exactly measured and calculated and are compiled in Tables 2, 3 and 4.

Zeta Potential Measurements. The electrophoretic mobility (U_e) of micellar solutions at volume fractions of $\phi=1\%$ were determined by a Malvern Zetasizer Nano ZS instrument. The solutions were adjusted to five different pH values, as shown in Table 4. Prior to measurements, the solutions were filtered by Whatman poly(ether sulfone) filters with 0.2 μ m pore size. The zeta potential ζ

Table 2. Experimental Volume Fractions (ϕ), pH-Values and Calculated Ionic Strength ([I]), of the Different C₂₈-PEO5-COOH and C₂₈-PEO5-OH Micelle Solutions Prepared for SANS Experiments

	C ₂₈ -PEO5-COOH pH 2			C ₂₈ -PEO5-COOH pH 6			C ₂₈ -PEO5-COOH pH 12			C ₂₈ -PEO5-OH
Sample ^a	ϕ^b (%)	pН	[I] ^c (mmol/L)	ϕ^b (%)	pН	[I] ^c (mmol/L)	ϕ^b (%)	pН	[I] ^c (mmol/L)	φ (%)
0.05	-	-	-	0.049	-	-	-	-	-	-
0.15	0.143	2.3	0.56	0.148	7.1	1.520	0.147	11.7	4.073	0.148
1	0.972	2.1	3.77	0.991	6.2	0.726	0.976	11.7	7.154	-
2.5	2.44	2.4	1.09	2.41	6.5	1.030	2.33	11.7	4.520	-
4	-	-	-	4.11	6.1 ^d	0.629	-	-	-	-
5	4.9	2.3	2.17	4.79	6.1^{d}	0.629	4.66	11.8	5.480	5.48
7.5	7.2	2.4^{d}	3.59	7.51	10.5 ^d	0.085	6.92	12.1 ^d	8.980	-
10	9.4	2.3^{d}	4.66	9.98	11.2 ^d	0.117	8.99	12.1 ^d	10.56	-

^aNominal volume fraction. ^bVolume fraction recalculated after pH adjustment. ^cFrom added HCl/NaOH and corrected for CO₂ absorption. ^dMacroscopically gelled at 20 °C.

Table 3. Experimental Volume Fractions (ϕ), pH-Values and Calculated Ionic Strength ([I]), of C₂₈-PEO5-COOH and C₂₈-PEO5-OH Micelle Mixtures

Sample ^a	ϕ^b (%)	pН	$[I]^c \text{ (mmol/L)}$
3:1	5.39	9.4	2.00
1:1	5.32	9.3	1.96
1:3	5.26	9.1 ^d	1.90

^aRatio of C₂₈-PEO5-OH: C₂₈-PEO5-COOH. ^bVolume fraction recalculated after pH adjustment. ^cFrom added HCl/NaOH solution and corrected for CO₂ absorption. ^dMacroscopically gelled at 20 °C.

Table 4. Zeta Potential^a (ζ), Viscosity^b (η), Ionic Strength^c ([I]) and Effective Number of Charges Z_{ep} of C₂₈-PEO5-COOH Solutions at ϕ = 1% and Different pH-Values

pН	2.4	3.3 ^d	6.2	10.3	11.8
ζ (mV)	-0.982	-12.2	-33.5	-21.5	-14.9
η (Pas)	1.509	1.726	2.2	1.836	1.66
[I] (mmol/L)	3.77	0	0.726	3.50	7.154
$ Z_{ep} $	1	20	66	59	49

^aCalculated from the electrophoretic mobility. ^bObtained by falling ball viscometry. ^cFrom added HCl/NaOH solution and corrected for CO₂ absorption. ^dpH of neat polymer solution at $\phi = 1\%$.

is calculated from the electrophoretic mobility using Henry's equation:

$$\zeta = \frac{3\eta}{2\varepsilon\epsilon_0 U_f(\kappa R)} \tag{1}$$

with η the sample viscosity and $\epsilon\epsilon_0=7.06\cdot 10^{-10}~{\rm AsV^{-1}m^{-1}}$ the permittivity of D₂O at 20 °C. $f(\kappa R)$ is Henry's function with κ^{-1} the Debye–Hückel length and R the particle radius. For $\kappa\cdot R\gg 1$, the Smoluchowski approximation can be used, and $f(\kappa R)=1.5$ in aqueous media. Exact viscosities of the 1% solutions at the different pH-values were determined using a Lovis M rolling ball viscometer of Anton Paar at 20 °C. Following the considerations of van Gruijthuijsen et al., ⁴⁸ the electrophoretic effective charge $Z_{\rm ep}$ can be estimated from the ζ -potential by

$$Z_{\rm ep} = \frac{\zeta}{z_{\rm e}} (4\pi\epsilon\epsilon_0 R_{\rm m} (1 + \kappa_{\rm s} R_{\rm m})) \tag{2}$$

Here $z_{\rm e}$ denotes the positive elementary charge. For the calculations, we have taken the micellar radius $R_{\rm m}$ for the particle radius R as obtained from SANS form factor analysis. A summary of the experimental and calculated values, respectively, is shown in Table 4.

Small Angle Neutron Scattering Experiments (SANS). Small angle neutron scattering (SANS) experiments were conducted at

archetypical pinhole geometry instrument D11 at Institut Laue-Langevin (ILL), Grenoble, France. Three sample to detector distances of 2, 8 and 28 m, and a neutron wavelength of $\lambda = 6$ Å were used. This configuration yields scattering data in the Q range 2.5 \times 10⁻³-0.47/Å, where $Q = (4\pi \sin(\theta/2))/\lambda$ denotes the scattering vector with θ as the scattering angle. The collimations were set identical to the sample to detector distances except for 2 m where the collimation was set to 4 m in order to avoid detector saturation. According to instrument specifications the installed velocity selector delivers neutrons with a wavelength spread of $\Delta \lambda / \lambda = 9\%$ (fwhm). Samples were measured in 404-QX Hellma quartz cells with 1 or 2 mm path length. A circular sample aperture was used with a 15 mm diameter. The experimental temperature was 20 °C. The scattering data were reduced according to standard instrument software taking into account corrections for detector sensitivity, electronic noise, and empty cell scattering. The reduced data were brought to an absolute scale by measuring the direct attenuated beam intensity. The obtained macroscopic differential scattering cross section $\frac{\mathrm{d}\Sigma}{\mathrm{d}\Omega}(Q)$ was subsequently corrected for solvent scattering and calculated incoherent contributions mostly originating from hydrogens of the unlabeled polymer chains.

SANS Data Modeling. Following previous works on the analysis of *n*-alkane-PEO block copolymer micelles by Zinn et al.⁴ and König et al.,³⁵ the scattering cross sections $\frac{d\Sigma}{d\Omega}(Q)$ are excellently modeled by

$$\frac{\mathrm{d}\Sigma}{\mathrm{d}\Omega}(Q) = \frac{\phi}{N_{\mathrm{agg}}(V_{\mathrm{C28}} + V_{\mathrm{PEO}})} [P(Q) \cdot S(Q) + I_{\mathrm{blob}}(Q)] \tag{3}$$

with ϕ the polymer volume fraction, $N_{\rm agg}$ the aggregation number and $V_{\rm C28}, V_{\rm PEO}$ the molar volume of core and corona block, respectively. P(Q) denotes a core—shell form factor for starlike micelles. Within this model, the n-alkyl core is considered as a compact sphere of radius $R_{\rm c}$ with constant density distribution. The PEO chains in the corona are highly swollen with water and exhibit a radially decaying density profile $\propto r^{-4/3}$, in agreement with theoretical predictions. It should be mentioned that we have not used the aspherical core—shell model introduced recently by König et al. 36 to account for the effect of n-alkyl chain packing because of neglibible contributions to the scattering profile under full contrast conditions. $I_{\rm blob}(Q)$ represents the so-called "blob" scattering originating from the internal structure of the coronal PEO chains and is added incoherently. The full analytical expressions of both P(Q) and $I_{\rm blob}(Q)$ can be found in refs 4 and 35. Data analysis and form factor fits were done with the open source software QtiSAS. 51

The intermicellar structure factor S(Q) observed at finite concentrations is due to direct interactions caused by steric or electrostatic repulsion between different micelles. Whereas the first results from inherent osmotic pressure between the polymeric corona (entropic interactions), the latter stems from tunable electrostatic Coulomb interactions between charges on the corona surface (enthalpic interactions). Which of them dominates structure formation and phase behavior in concentrated solutions crucially

depends on the given molecular/experimental parameters like molar mass of the PEO block, aggregation number, pH value, ionic strength, etc.

For the liquid phase, i.e., for distances r larger than the particle diameter $2R_{\rm mr}$ steric and electrostatic repulsion can both be described by a screened Yukawa-type potential $U(r) \sim (1/r) \cdot \exp(-\kappa r)$. Its explicit form and quantitative relation to molecular/experimental parameters is given in the Appendix and described in detail in the literature. ^{3,31} Using standard liquid state theory, the direct correlation function g(r) and its Fourier transform S(Q) can be calculated and finally compared to experimental SANS data. The challenging task is to relate all crucial parameters of the interaction potential unambiguously to experimental parameters given by the samples.

The crossing of the liquid—solid phase boundary typically occurs at intermicellar distances r close to $\approx 2R_{\rm m}$. For smaller r the archetypical potential for charged stabilized colloids assumes "Hard Sphere"-like interactions, i.e. an impenetrable sphere with radius $R_{\rm HS} \approx R_{\rm m}$. For sterically stabilized colloids, where diffuse polymeric coronae can substantially overlap, a logarithmic potential $U(r) \sim -\ln(r)$ for r smaller than $\approx 2R_{\rm m}$ is proposed. In the solid regime, the decoupling of P(Q) and S(Q) is no longer strictly valid due to increasing three body forces but still reasonably describes data in the amorphous glass phase. In the crystalline phase, we restrict our analysis of SANS data to the identification of the crystal structure and an evaluation of the corresponding lattice parameters.

RESULTS AND DISCUSSION

Zeta Potential and Electrophoretic Effective Charge. The zeta potential ζ and the viscosity η of C₂₈-PEO5-COOH solutions at $\phi = 1\%$ in D₂O at different pH-values are shown in Figure 4. As expected, ζ is almost zero at pH 2 indicating that

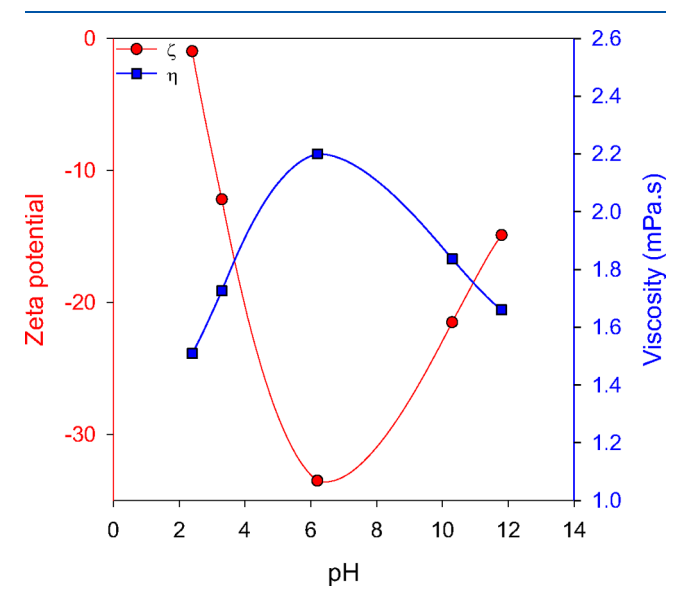


Figure 4. Zeta-potential ζ and viscosity η of C₂₈-PEO5-COOH solutions at $\phi = 1\%$ in D₂O for different pH-values. Solid lines are guides to the eye.

the carboxy groups are not dissociated, and micelles are electrically neutral. With increasing pH, the zeta potential drops rapidly to a minimum value of -33.5 mV around pH 6 and increases again to higher values at higher pH. The opposite trend is observed for the viscosity with a maximum around pH 6.

To rationalize these findings, we have to consider that below the equivalence point, all added NaOH reacts in a classical neutralization reaction with the carboxy groups forming H_2O and $C_{28}\text{-PEO5-COO}^ Na^+$. At the equivalence point, all carboxy groups are dissociated/deprotonated. We thus observe at low pH an increasing number of surface charges up to (nominally) N_{agg} and, consequently, an increasing absolute value of the zeta-potential. In this range, however, the number of ions and thus the ionic strength stays constant. Above the equivalence point, added NaOH increases further the pH but additionally acts as a "simple" 1:1 electrolyte leading to a larger number of ions in solution and thus to a higher ionic strength [I]. Hence, κ and screening of electrostatic interactions increase, while all carboxy groups are dissociated. Therefore, the absolute value of ζ decreases according to eq 1. From the zeta-potential, the electrophoretic effective charges were calculated by eq 2 ranging from $Z_{\rm ep} \approx$ 0 at pH 2 to a maximum value of $Z_{\rm ep} \approx 66$ at pH 6 before it decreases again to $Z_{\rm ep} \approx 49$ at pH 11.8.

The observed maximum in viscosity is a direct consequence of the maximum in $Z_{\rm ep}$. Although at a polymer volume fraction of only $\phi=1\%$, samples can be considered to be already in the concentrated regime in case electrostatic interactions are effective. This is corroborated by the structure factor analysis discussed subsequently.

Small Angle Neutron Scattering. Small angle neutron scattering data of C_{28} -PEO5-COOH are shown in a double logarithmic representation in Figure 5 for different pH-values and concentrations. The scattered intensity $\frac{d\Sigma}{d\Omega}(Q)$ in absolute units (cm^{-1}) is normalized by the respective volume fractions ϕ . The fact that the data fall on top of each other at high Q values for all pH-values is a direct proof of precise sample preparation and data correction. Furthermore, it reflects the same intramicellar structure at small length scales ("blob scattering" due to excluded volume interactions) without any biasing fitting procedure.

At low Q, one observes for all pH values a decrease of the intensity with concentration and simultaneously the evolution of a correlation peak at intermediate Q. This is a typical sign of increasing structure factor contributions arising from intermicellar interactions. There are however significant differences for the different pH-values. At pH 2, where micelles are uncharged, for the lowest concentration at $\phi = 0.15\%$ the scattered intensity solely stems from the form factor of the starlike micelles, i.e. $S(Q) \approx 1$. At higher volume fractions at ϕ = 1%, 2.5% and ϕ = 5% the scattering pattern suggests a liquid like order arising from soft colloidal interactions due to steric repulsion analogous to the behavior of C₂₈-PEO5-OH micelles studied previously.³³ At $\phi = 7.5\%$, higher-order Bragg peaks occur, indicating a transition to a crystalline structure. At pH 6 on the other hand the concentration dependence of the scattering pattern significantly differs from that at pH 2. Here, $\frac{d\Sigma}{d\Omega}(Q)$ displays a pronounced structure factor peak even at the lowest volume fraction at ϕ = 0.15%, a liquid like structure at ϕ = 1% and 2.5% and the onset of a crystalline order already at a significantly lower volume fraction of ϕ = 4%. We relate this behavior to stronger interactions due to long-range electrostatic repulsion between the micelles now bearing a surface charge that reaches a maximum at pH 6. The concentration dependence of the scattering curves at pH 12 is similar to pH 2 except for the scattering curve at the lowest concentration where a shallow peak is still present at intermediate Q. According to the zeta-potential results, the electrostatic repulsion between charged micelles is mitigated at higher pH values because of the higher ionic strength resulting from the

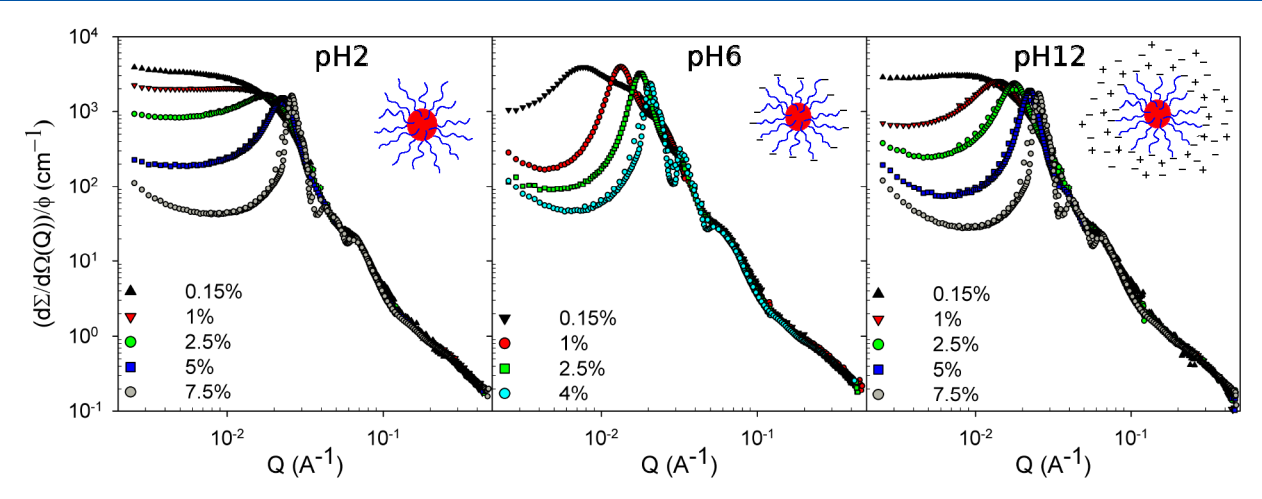


Figure 5. Macroscopic scattering cross-section $\frac{d\Sigma}{d\Omega}(Q)$ vs scattering vector Q of C₂₈-PEO5-COOH in D₂O at pH 2, 6, and 12 normalized by polymer volume fraction ϕ for various concentrations in the dilute to semidilute region. Numbers denote nominal polymer volume fraction in %.

addition of NaOD for pH adjustment. In the following, we will analyze the SANS curves in more detail by dividing our approach into form factor analysis at low volume fractions and structure factor analysis in the liquid and crystalline state for intermediate and high concentrations, respectively.

Form Factor Analysis. Figure 6 (top) shows SANS curves of C_{28} -PEO5-OH (black) and C_{28} -PEO5-COOH at pH 2 (red) at the lowest measured concentration at $\phi = 0.15\%$ in D_2O . Within experimental error bars the two data sets are identical over the whole measured Q-range when normalized

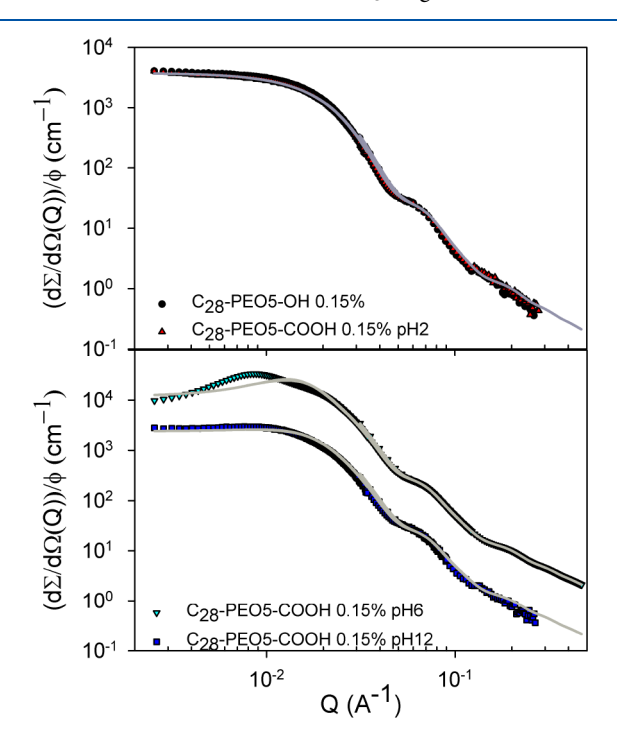


Figure 6. (top) Comparison of scattering curves of uncharged micelles at $\phi=0.15\%$ formed by C₂₈-PEO5-OH and C₂₈-PEO5-COOH at pH 2 in D₂O. Solid line represents the core—shell form factor fit (data are normalized by volume fraction). (bottom) Comparison of scattering curves at $\phi=0.15\%$ of C₂₈-PEO5-COOH at pH 6 (data multiplied by 10) and pH 12, solid lines are fits to the core—shell form factor P(Q) coupled with the classical Hayter-Penfold approach for S(Q), see text.

to the volume fraction ϕ . Without any further quantitative analysis, this directly indicates that the -COOH end group in the undissociated state, i.e., $Z \approx 0$, has no effect on single micellar properties and intermicellar interactions.

From previous analysis of SANS data of C_n-PEO-OH micelles, it is known that for dilute solutions at $\phi \leq 0.25\%$, structure factor contributions resulting solely from steric interactions are negligible.4 Accordingly, the scattering data were analyzed by eq 3 with S(Q) = 1 and P(Q) the spherical core-shell form factor described in section "SANS data modeling". The scattering data were fitted as earlier reported in detail by Zinn et al.4 Since both SANS curves are basically identical, a simultaneous fit was performed yielding a common set of parameters. The fit is shown as solid line in Figure 6 (top). Fixed parameters were the given experimental volume fraction ϕ , the molar volumes of core $V_{\rm C28} = M_{\rm C28}/d_{\rm C28}$ and corona block $V_{\rm PEO}$ = $M_{\rm PEO}/d_{\rm PEO}$, respectively, with $M_{\rm C28}$ = 393 g/mol the molar mass of the octacosyl block and $M_{\rm PEO}$ = 4997 g/mol the molar mass of PEO (NMR-result, see Table 1). The corresponding densities are $d_{C28} = 0.9 \text{ g/cm}^3$ for partially crystalline octacosyl chains³⁵ and $d_{\rm PEO}=1.196~{\rm g/cm^3}$ the density of PEO in the micellar state.⁵² The total coherent scattering lengths of the two blocks and the solvent $\sum b_{C28}$ = -2.712×10^{-12} cm, $\sum b_{PEO} = 4.73 \times 10^{-11}$ cm and $\sum b_{\rm D_2O} = 1.914 \times 10^{-12} {\rm cm}$ were calculated and also fixed. The internal parameters, effectively controlling the mid to high Q-range, were the blob size of the PEO chain $R_g = 46$ in the corona, the smearing of the core/corona interface $\sigma_{int} = 2 \text{ Å}$, and the relative smearing of the outer corona $\sigma_{\rm out}$ = 0.12. These parameters are slightly adjusted values of a previously performed analysis⁴ and were fixed in the final fit. The only remaining parameters to be fitted are the aggregation number $N_{\rm agg} = 145 \pm 5$ and the micellar radius $R_{\rm m} = 125(5)$ Å. The core radius $R_c = 29(1)$ Å is coupled to N_{agg} and calculated by $N_{\text{agg}} \cdot V_{\text{C28}} = \frac{4\pi}{3} R_{\text{c}}^3$ assuming a spherical core of densely packed partially crystalline octacosyl chains. All fit parameters describing micellar form factor P(Q) are summarized in Table 5.

Figure 6 (bottom) compares SANS curves of C_{28} -PEOS-COOH solutions in D_2O at $\phi = 0.15\%$ at pH 6 and pH 12. The scattering profiles of the two solutions overlap perfectly at $Q > 0.02/\text{Å}^{-1}$ with the calculated form factor. This implies that

Table 5. Compilation of Micellar Parameters Obtained by Simultaneous Core/Shell Form Factor Analysis of SANS Data of -COOH-terminated Polymer at pH 2 and -OH-terminated Polymer at $\phi = 0.15\%$

$N_{ m agg}$	R_m (Å)	R_c (Å)	$R_{\rm g} (\rm \mathring{A})^a$	$\sigma_{ m int}$ (Å)	$\sigma_{ m out}$		
145 ± 5	125 ± 5	29 ± 1	46	2	0.12		
^a Radius of gyration of PEO chain							

the structure of a single micelle does not change with pH, or strictly speaking, with the number of surface charges on the periphery of the micelles. In contrast to charged soft colloids based on polyelectrolytes (PE) as PE block copolymer micelles, PE stars, PE dendrimers, and PE microgels, the corona swelling as a function of ionic strength and/or pH is minimized due to the localization of charges only at the corona chain end. Significant deviations, however, are observed at Q < 0.02/Å⁻¹. In this range, the scattered intensity decreases, and a correlation peak develops due to the presence of surface charges. The resulting electrostatic repulsion lead to long-range interactions, such that the micelles at $\phi = 0.15\%$ are no longer in the dilute regime and structure factor contributions need to be considered in the SANS data analysis. (Note: It should be mentioned that a test measurement of a further diluted sample at pH 6 at $\phi \simeq 0.05\%$ still shows significant structure factor contributions at low Q. Because of the low scattering intensity we relinquished from accurate measurements on more diluted samples.) As expected, the electrostatic interactions are most pronounced at pH 6 at which the number of electrophoretic effective charges $Z_{\rm ep}$ was found to be maximum (see Table 4 and related discussion in section "Zeta Potential Measurements").

In a first approach, a simple model coupling the described core—shell form factor P(Q) and the classical Hayter—Penfold approach for the structure factor S(Q) of charged spheres^{53,54} has been used to fit scattering curves at pH 6 and pH 12. Additional parameters used in S(Q) are the effective charge Z_{eff} , the hard sphere radius R_{HS} , the corresponding hard sphere volume fraction ϕ_{HS} , and the ionic strength [I]. Using R_{HS} = $R_{\rm m}$ and calculating $\phi_{\rm HS}$ from the given experimental number density of micelles N_z as well as [I] unambigously given by sample composition, the only parameter to be fitted remains Z_{eff} . The best fit was obtained for pH 12 with an effective charge of 30 and with fixed parameters for the form factor as obtained from a simultaneous analysis of C28-PEO5-OH and C₂₈-PEO5-COOH at pH 2 (see Table 5). A reasonable fit can also be obtained for pH 6, interestingly also with an effective charge of 30, but the R_{HS} of 290 Å instead of 125 Å does not seem physically reasonable. Moreover, all fit curves only provide a marginally better description of our experimental data; therefore, we show as solid lines in Figure 6 (bottom) those with all parameters fixed to experimental values including $Z_{\rm eff}$ = $Z_{\rm ep}$ = 66. For higher concentrations $\phi \gg$ 0.15%, an experimental S(Q) can be extracted from the scattering intensity. This provides a much larger and more precise data set, and therefore, we discuss a detailed analysis of S(Q) as a function of concentration by a more elaborate theoretical model separately in the next section.

Structure Factor Analysis. In this section, we focus on the analysis of samples at pH 6 and pH 12, where all carboxy groups are dissociated and electrostatic interactions play an important role. The difference lies in the ionic strength which varies from ≈ 0.7 mmol/L at pH 6 to ≈ 7.0 mmol/L at pH 12.

We start the structure factor analysis by calculating theoretical S(Q) for the liquid phase. These are solely based on given, precisely defined experimental parameters. Without any fitting procedure we compare the calculated S(Q) to our experimental data and check how observed experimental results coincide with expected theoretical predictions. For the crystalline phase, we restrict our analysis to the characterization of the observed crystal structure and corresponding lattice parameters.

Structure Factor in the Liquid State. Using liquid state theory, S(Q) can be calculated from the Ornstein–Zernike equation and an appropriate closure relation. We choose the modified penetrating background corrected rescaled mean spherical approximation (MPB-RMSA) of Heinen et al.,³¹ an established and frequently used theoretical approach.^{48,55} This approach is shortly summarized in the Appendix, but for details, we refer the interested reader to the original literature.

As can be seen in Figure 6, for $Q \leq 0.1\,\text{Å}^{-1}$ the blob scattering in eq 3 can be neglected. The amplitude normalized to volume fraction $\frac{\mathrm{d}\Sigma}{\mathrm{d}\Omega}(Q)/\phi$ of the blob scattering is small $\approx 20~\mathrm{cm}^{-1}$ compared to a total amplitude of $\approx 3300~\mathrm{cm}^{-1}$ and to the amplitude of the micellar core of $\approx 47~\mathrm{cm}^{-1}$ (see also Figure S1 in the SI). Therefore, the experimental scattering curves $\frac{\mathrm{d}\Sigma}{\mathrm{d}\Omega}(Q)$ were divided by the previously determined form factor P(Q) to extract the experimental structure factors, with $S(Q) \propto \frac{\mathrm{d}\Sigma}{\mathrm{d}\Omega}(Q)/P(Q)$. Structure factors at different pH values and concentrations in the liquid regime are shown in Figure 7.

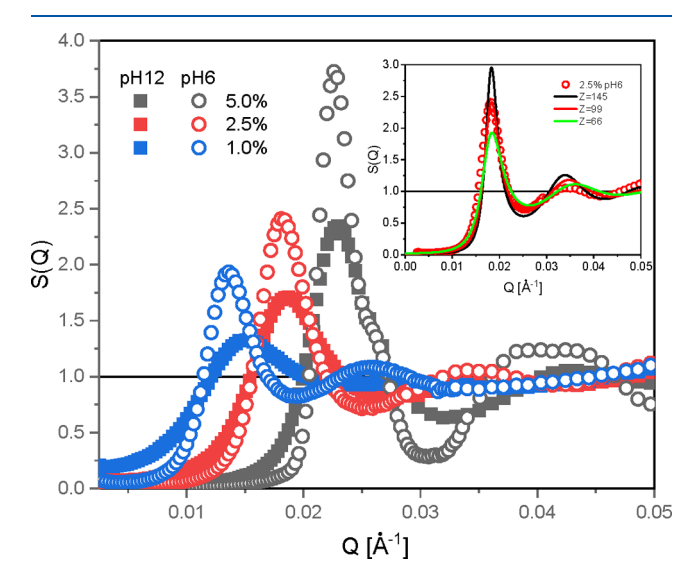


Figure 7. Experimental structure factors as a function of volume fraction ϕ , pH 6 (lines) and pH 12 (symbols). The sample with ϕ = 5% at pH 6 is already in the solid regime, all other samples are liquids. Inset: Comparison between experiment (symbols) and theory (lines) for ϕ = 2.5% at pH 6 (see text).

For all volume fractions $\phi \geq 1\%$ a distinct main peak can be observed and even secondary and tertiary peaks appear at higher concentrations. When the concentration increases, the main peak position $Q_{\rm max}$ is shifted to the larger Q vectors. $Q_{\rm max}$ reflects the intermicellar distance $D \sim 2 \cdot \pi/Q_{\rm max}$ and its shift is the signature of the decreasing distance between micelles with an increasing concentration. The peak position $Q_{\rm max}$ does not vary significantly when the pH is changed, implying that the intermicellar distance is pH independent. Small differences

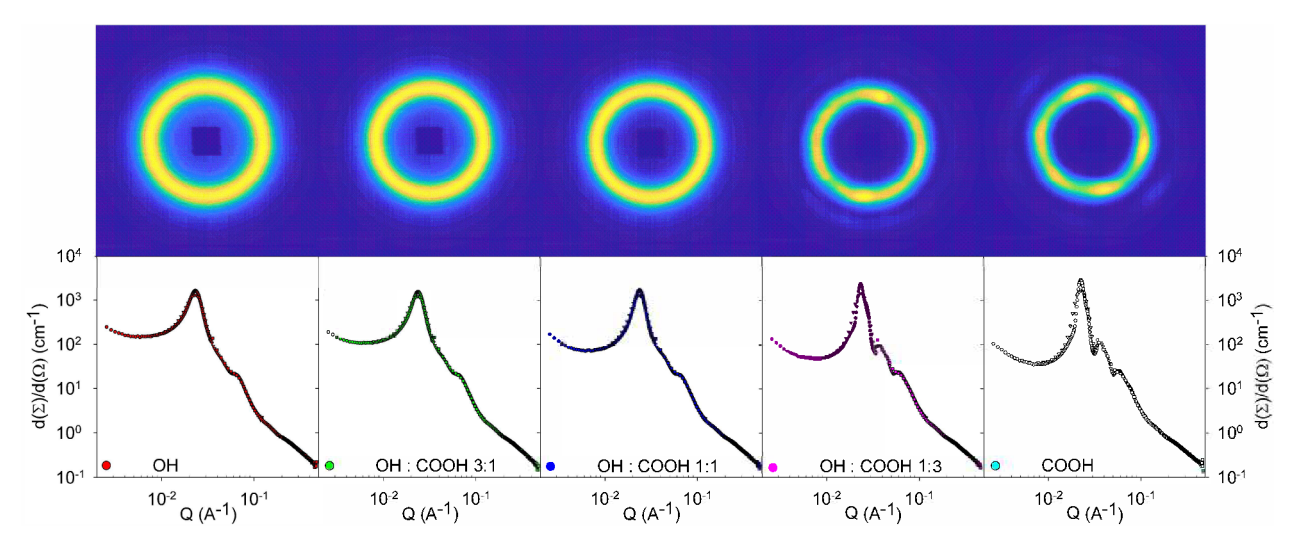


Figure 8. 2D SANS images (top), and SANS scattering curves (bottom) of micellar solutions in D_2O of mixtures of -OH and -COOH terminated polymers at different mixing ratios (indicated in the figure) at pH 6 and a total polymer volume fraction of $\phi = 5\%$.

observed at different pH values are attributed to the variation of the experimental volume fraction (shown in Table 2). Since form factor analysis revealed a pH independent micellar radius $R_{\rm m}$ as well as a pH independent internal structure of the single micelle (see section "Form factor analysis"), a constant peak position $Q_{\rm max}$ can be expected.

But for the same concentration, the structure factor peak is always substantially higher at pH 6 than pH 12 due to the stronger electrostatic interactions which leads to more pronounced long-range ordering.

The structure factor can be fitted by the MPB-RMSA model with effective charge Z_{eff} as the only fitting parameter. Fixed parameters are the ionic strength [I] and corresponding κ , the micellar volume fraction $\phi_{\rm HS}$, the micellar radius $R_{\rm m}$, and the solvent dielectric constant given by the experimental values. Two limiting values for $Z_{\rm eff}$ are obvious, the lowest limit being the electrophoretic charge $Z_{\rm ep} = 66$ (for pH 6) and $Z_{\rm ep} = 49$ (for pH 12) whereas the highest limit $Z_{\rm max} = N_{\rm agg} = 145$ is given by the aggregation number. Since each copolymer chain carries only one ionizable function, the number of charges cannot be larger than the aggregation number. The two limiting S(Q)were calculated and are exemplary shown for ϕ = 2.5% at pH 6 in the inset of Figure 7. Also shown is the best fit obtained with a number of charges of $Z_{\rm eff}$ = 99. The agreement between experiment and theory is promising, in particular if theoretical S(Q) are shifted along the Q-axis by a factor of only 6% which is within experimental errors for $R_{\rm m}$.

Structure Factor in the Solid State. For all pH values, macroscopic freezing of samples with increasing concentration is observed. The liquid—solid transition is confirmed by rheology where the elastic modulus *G'* is always larger than the loss modulus *G''* over the entire frequency range (see SI). Simultaneously with macroscopic freezing, Bragg reflections appear in the 2D detector data, indicating unambiguously the presence of a crystalline phase. The radially averaged data of all solid samples show strong structure factor peaks, which have higher intensity and are sharper than in the liquid regime. Higher order peaks up to the fifth order become visible (see Figure 5).

The phase transition at pH 2 and 12 occurs at $\phi = 7.5\%$ while the crystalline phase at pH 6 already appears at a much lower concentration at $\phi = 4\%$. All crystalline samples fulfill the

Hansen-Verlet criterion which predicts frozen systems when $S(Q)_{\text{max}} \ge 2.85.^{56}$ An exception is the 4% sample at pH 6 which is crystalline but shows a main peak smaller than 2.85. This apparent contradiction is explained by the resolution of the SANS data significantly reducing the height of $S(Q_{max})$. As in the liquid regime, the main peak is shifted to larger Q values, and the intensity of the main peak increases with concentration. The crystalline structure can be determined from the position of the higher order peaks, knowing that the most probable phases, according to the theoretical phase diagram, are face centered cubic (fcc) and body centered cubic (bcc) at those intermediate concentrations. Higher order crystalline peaks correspond to the theoretical values for an fcc structure for all samples at all pH: $a\sqrt{(4/3)}$, $a\sqrt{(8/3)}$, $a\sqrt{(12/3)}$ and $a\sqrt{(19/3)}$ with a the position of the maximum of the main peak.

Mixtures of Uncharged (-OH) and Charged (-COOH) **Polymers.** Adjusting a small number of surface charges, $Z_{\text{eff}} \ll$ Z_{max} by a lower degree of dissociation and/or by variation of pH is challenging, in particular, for pH-values below the equivalence point (pH 7.9). In this range the degree of dissociation depends additionally on concentration such that for weak acids a systematic study at a constant number of surface charges per micelle is almost impossible. Yet, to further fine-tune the number of surface charges we have used mixtures of C₂₈-PEO5-OH and C₂₈-PEO5-COOH at pH 6 in a 3:1, 1:1 and 1:3 ratio at an overall volume fraction ϕ = 5%. At pH 6 all ionizable groups are dissociated, and we know exactly the maximum number of charges Z_{max} per micelles due to the given mixing ratio. Radially averaged scattering curves show a transition from the liquid state to an fcc crystalline structure. The same transition can be observed in the 2D data, by the appearance of Bragg peaks on the Debye-Scherrer rings. The liquid-crystal transition occurs between mixing ratios 1:1 and 1:3, i.e., approximately between Z_{max} = 72 and Z_{max} = 108 (or between $Z_{\rm eff}$ = 50 and $Z_{\rm eff}$ = 75, respectively) as shown in Figure 8.

Figure 9 shows exemplarily the corresponding experimental and calculated theoretical S(Q) for 1:1 mixtures at pH 6. This mixing ratio gives an expected $Z_{\rm eff} = 50$, and the observed agreement between experiment and theory is again convincing.

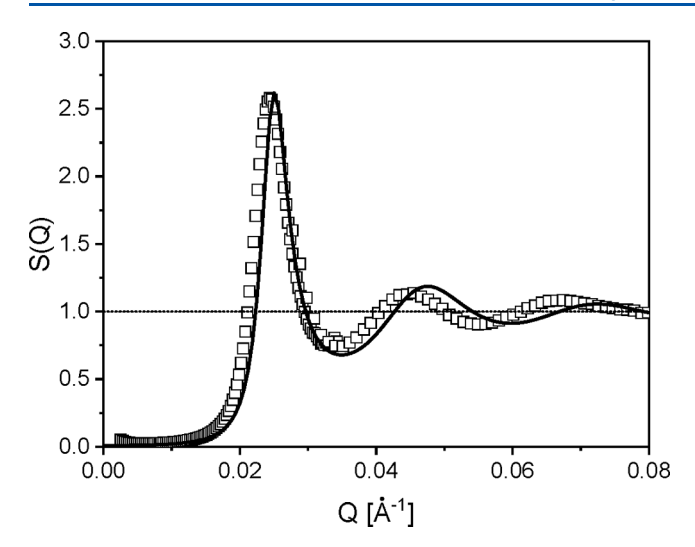


Figure 9. Comparison of experimental and calculated (solid line) S(Q) for a mixture of C_{28} -PEO5-OH and C_{28} -PEO5-COOH polymers with a mixing ratio 1:1 at $\phi = 5\%$ and pH 6.

Therefore, mixing uncharged (-OH) and charged (-COOH) polymers is a "smart" way to adjust even a small number of surface charges, a regime which is important for many classes of soft colloids. Even PMMA-colloids¹³ or PNIPAM- μ -gels³⁰ exhibit weak electrostatic interactions. These systems have been thought for a long time to be uncharged, but both contain a small number of residual charges from chemical synthesis.

Phase Diagram. The experimental phase diagram of all investigated samples including mixtures is shown in the ϕ , pH representation in Figure 10 left. Here open symbols denote liquid and closed symbols solid samples (all fcc). The solid line is a guide-to-the-eye to illustrate the liquid-solid phase boundary. The liquid-solid transition was confirmed by additional rheology experiments as crossover from G'' > G'to G' > G'' (see SI). We want to point out that all solid samples were crystalline, no amorphous "gel-like" or glassy samples were observed in contrast to many similar systems stabilized by pure steric repulsion.^{7,9} Puaud et al. reported the general importance of fast unimer exchange dynamics to achieve the equilibrium crystalline state for micelles formed by amphiphilic block copolymers, 57 which is consistent with our findings. Obviously, for our C_{28} -PEO5-COOH micelles, the liquid solid transition is shifted to lower volume fractions when the electrostatic interactions remain unscreened at pH 6 as already

discussed in the previous sections. To rationalize the experimentally observed concentration and pH dependence of S(Q) and to quantify its comparison with theory, we have to consider several characteristic length scales as illustrated in Figure 3.

- the particle radius $R \approx R_{\rm m}$,
- the mean geometrical distance between charges on the surface of a single particle $D_{\rm charge} \approx \sqrt{4\pi R_{\rm m}^2/N_{\rm agg}}$
- the mean geometrical distance between particles $D \approx N_{\pi}^{-3}$, with N_z the micellar number density.
- the Debye–Hückel screening lengths κ^{-1} (see eq 7).

 $R_{\rm m}=125~{\rm Å}$ and $D_{\rm charge}=37~{\rm Å}$ are constant, whereas D and κ^{-1} depend on concentration and ionic strength [I]. The starting value is $D=9~{\rm Å}\approx 8R_{\rm m}$ in dilute solution at $\phi=0.15\%$ which decreases to $D=225~{\rm Å}\approx 2R_{\rm m}$ at the highest concentration at $\phi=10\%$. The corresponding Debye–Hückel screening length κ^{-1} decreases from $\approx 74~{\rm Å}$ at $\phi=0.15\%$ to $\approx 19~{\rm Å}$ at $\phi=10\%$ at pH 6 and from $\approx 47~{\rm Å}$ to $\approx 20~{\rm Å}$ at pH 12. In addition, we calculated the overlap volume fraction ϕ^* at

In addition, we calculated the overlap volume fraction ϕ^* at which micelles are in direct contact by

$$\phi^* = \frac{N_{\text{agg}} V_{\text{C28-PEO5}}}{N_{\text{A}}} / \left(\frac{4}{3} \pi R_{\text{m}}^3\right)$$
 (4)

where $V_{\rm C28\text{-}PEO5}$ is the molar volume of the polymer and $N_{\rm A}$ Avogadros number. Taking $R_{\rm m} = 125 \,\text{Å}$ from the form factor analysis we calculated for our micelles $\phi^* \approx 14\%$. Irrespective of the number of surface charges, we however observe crystallization at much lower concentrations than ϕ^* for all investigated pH-values. To take all concentration dependencies into account more quantitatively, a reduced phase diagram is constructed from the parameters given by the sample composition and obtained from the structure factor analysis. Using the mean geometrical distance between colloids $D = N_z^{-3}$, reduced potential parameters $\tilde{\gamma} = \gamma 2R_m/D$ and $\tilde{\kappa} = \kappa D/(2R_m)$ can be defined as well as a reduced temperature $\tilde{T}=e^{\tilde{\kappa}}/\tilde{\gamma}$. Here $\gamma=l_{\rm B}Z_{\rm eff}^2\Big(\frac{e^{\kappa R_{\rm HS}}}{1+\kappa R_{\rm HS}}\Big)^2$ is the amplitude or prefactor of the Yukawa potential defined in eq 6. The reduced phase diagram in the \tilde{T} , $\tilde{\kappa}$ representation is shown in Figure 10 right. The experimental error bars result from uncertainty in the ionic strength and effective charge. The theoretical melting line as predicted by Kremer et al.⁵⁸ is

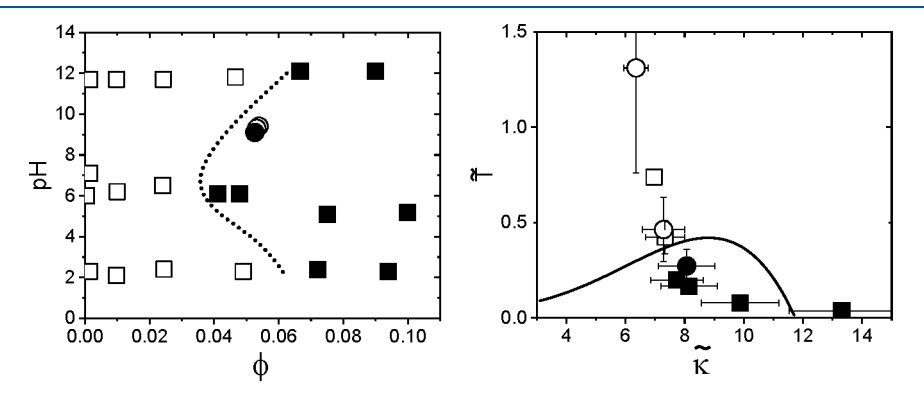


Figure 10. left: Experimental phase diagram in the ϕ ,pH-representation, the dotted line is a guide-to-the-eyes, right: Reduced phase diagram for pH 6 in the \tilde{T} , \tilde{K} representation, see text. Open symbols denote liquid, closed symbols fcc crystalline samples, and circles mixtures. The solid line is the theoretical melting line. ^{31,58}

shown as a solid line. This reduced phase diagram allows a direct comparison between experiment and theory. At least for pH 6 a reasonable agreement for the phase boundary is observed; however, for other pH-values, huge experimental error bars are obtained and the agreement becomes worse (data not shown). Nevertheless, when keeping in mind that the only adjustable parameter used to generate the reduced phase diagram is the effective charge $Z_{\rm eff}$ from analysis of S(Q) and all other parameters are fixed starting from unambiguous experimental values, the agreement is reasonable.

CONCLUSION

Surface charged micelles formed by carboxy terminated noctacosyl-poly(ethylene oxide) block copolymers, C_{28} -PEOS-COOH with 5 the PEO molar mass in kg/mol of the PEO block, are appropriate model systems for charge stabilized colloids. The main advantage is the relative control of the number of surface charges and its relation to microscopic structural parameters unambiguously given by sample composition ("tunability"). In aqueous solution, the micellar surface charge can be varied from 0 to the maximum possible number of surface charges $Z_{\rm max} = N_{\rm agg}$ by adjusting the pH relative to p $K_{\rm a}$. By using mixed micelles of oxidized (-COOH) and nonoxidized block copolymers (-OH) $Z_{\rm max}$ can be further controlled by the stoichiometric mixing ratio. The surface charges on these micelles introduce electrostatic interactions in addition to the inherently present steric repulsion.

Micellar solutions of C28-PEO5-COOH (-OH) were investigated at different concentrations, pH-values, ionic strengths, and mixing ratios by SANS, zeta potential measurements, and rheology. By accurately analyzing the intramicellar form factor P(Q) we found that the structure of the individual micelles is not affected by the presence of surface charges. On the contrary the intermicellar structure factor S(O) and the phase behavior show a strong dependence on the number of surface charges. Both were quantitatively analyzed in terms of screened Hard Sphere Yukawa potential. Starting from parameters given by the microscopic structure of the individual micelle and sample composition, we found very good agreement between experiment and theory using almost no adjustable parameter. In particular, we observe a strong dependence of the liquid - fcc crystal phase boundary on the number of effective surface charges. Therefore, we propose our micelles as a model system to further investigate the competition between steric and electrostatic interactions in colloidal solutions.

As an outlook for future work, we want to point out that our system is a hybrid in several ways. First, with respect to the "tunability" of the number of surface charges, it bridges not only between sterically and charge stabilized colloids but also between neutral polymer and polyelectrolyte block copolymer micelles as well as between nonionic and ionic surfactant micelles. Second, it interconnects colloids, block copolymer micelles, and surfactant micelles. As for most block copolymer systems, the PEO block length can be adjusted and additionally offers a "tunability" in size. Finally, we can easily control the activation energy for unimer exchange by adjusting the molar mass of the hydrophobic (*n*-alkane) block, which allows us to switch between kinetically "frozen" and "living" surface charged polymeric micelles.

To summarize, such "tunable soft colloids" can be considered as a very versatile hybrid material connecting properties of a variety of different classes of synthetic systems.

These may even bridge the gap to biological materials where surface charges for instance determine the structure, function, and solubility of proteins.

■ APPENDIX - EFFECTIVE POTENTIALS AND RELATED EXPERIMENTAL PARAMETERS

The effective potential³ for regular star polymers, and more general for sterically stabilized ultrasoft colloids, separated by a distance r is given by

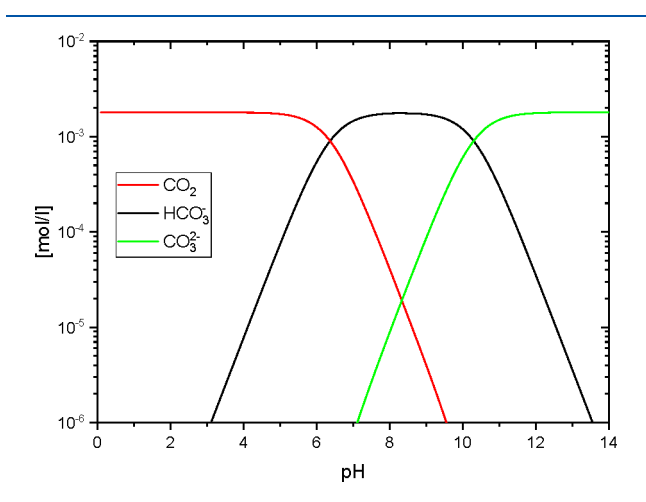


Figure 11. Bjerrum plot showing the concentrations of ionic species from CO_2 absorption as a function of pH.

Table 6. Concentration of (Micro)Ions and Resulting Ionic Strength of C_{28} -PEO5-COOH-Solutions in mmol/L Taking into Account CO_2 Absorption

ϕ^a	pН	c_{-COOH}	c_{HCO_3}	$c_{\text{CO}_3^2}$	$[I]^b$
0.15	7.1	0.316	1.52	$9.57 \cdot 10^{-4}$	1.520
1.00	6.2	2.118	0.73	$5.77 \cdot 10^{-5}$	0.726
2.50	6.5	5.153	1.03	$1.64 \cdot 10^{-4}$	1.030

^aNominal volume fraction in %. ^bCalculated by eq 8.

$$\beta U(r) = \begin{cases} \frac{5}{18} f^{3/2} \left[-\ln\left(\frac{r}{\sigma}\right) + \frac{1}{1 + \sqrt{f}/2} \right] & r \le \sigma \\ \frac{5}{18} f^{3/2} \frac{\sigma}{1 + \sqrt{f}/2} \frac{e^{[-\sqrt{f}(r-\sigma)/2\sigma]}}{r} & r \ge \sigma \end{cases}$$
(5)

with $\beta=1/k_{\rm B}T$, f the number of arms, and σ the star diameter. For star-like micelles $f=N_{\rm agg}$ and $\sigma\approx 2R_{\rm m}$.

The potential U(r) resulting from electrostatic interactions between charge stabilized colloids with hard sphere radius $R_{\rm HS}$ and effective charge $Z_{\rm eff}$ can be described by a screened Yukawa form:³¹

$$\beta U(r) = \begin{cases} \infty & r \le 2R_{\rm HS} \\ l_{\rm B} Z_{\rm eff}^2 \left(\frac{e^{\kappa R_{\rm HS}}}{1 + \kappa R_{\rm HS}} \right)^2 \frac{e^{-\kappa r}}{r} & r > 2R_{\rm HS} \end{cases}$$
 (6)

All prefactors can be combined as $\gamma = l_{\rm B} Z_{\rm eff}^2 \left(\frac{e^{\kappa R_{\rm HS}}}{1+\kappa R_{\rm HS}}\right)^2$. Here, $l_{\rm B}$ is the Bjerrum length with a value of 7.1 Å in water at

T = 20 °C. The screening parameter κ is given by

Macromolecules Article pubs.acs.org/Macromolecules

$$\kappa = \sqrt{l_{\rm B} \left(\frac{3\phi_{\rm HS} Z_{\rm eff}}{R_{\rm HS}^3 (1 - \phi_{\rm HS})} + 8\pi [I] N_{\rm A} \right)}$$
 (7)

 κ has the dimension of an inverse length, therefore κ^{-1} is also known as Debye-Hückel length and describes the range of electrostatic interactions. The first term in eq 7 results from counterion release of the colloidal (macro)ion whereas the second summarizes all other (micro)ions (e.g., by additional salt or buffer etc.) present in solution excluding those from the ionized colloidal particles themselves. The so-called ionic strength [I] is defined by

$$[I] = \frac{1}{2} \sum c_i z_i^2 \tag{8}$$

Here c_i is the concentration of (micro)ion of species i in mol/L with charge z_i . It is important to note that only for 1:1 electrolytes the ionic strength [I] is identical to the total salt concentration $c_s = \sum c_i$.

Since we were aiming to maximize electrostatic interactions we used no additional salt nor buffer, all ions present in solution solely stem from the block copolymer and added acid HCl or base NaOH to adjust the pH. To calculate the ionic strength from experimental values, we have to take into account the following two chemical reactions, which affect the total number of ions present in the solution.

a. The reaction between the terminal carboxy group (a weak acid) of the block copolymer and sodium hydroxide (a strong

$$C_{28}$$
-PEO5-COO $^{-}$ H⁺ + Na⁺OH $^{-}$
 $\rightarrow C_{28}$ -PEO5-COO $^{-}$ Na⁺ + H₂O

This neutralization reaction takes place instantaneously, is irreversible and therefore reduces the number of ions since H⁺ and OH are recombining to H₂O.

For practical reasons we worked in addition at ambient pressure ("open samples") and together with the absence of additional salt/buffer ("no electrostatic background", i.e. low ionic strength) we have to consider:

b. The absorption of atmospheric CO₂ by our samples and corresponding dissociation reactions in the solutions:

$$CO_2(g) \rightleftharpoons CO_2(aq) \rightleftharpoons H_2CO_3 \rightleftharpoons H^+ + HCO_3^-$$

 $\rightleftharpoons 2H^+ + CO_3^{2-}$

The amount of each species in these reactions series depends on pH and can be quantified by the known dissociation constants/p K_a values. We combined an approach described by Kang et. al⁵⁹ and reference data given by Zeebe and Wolf-Gladrow.⁶⁰ Using p $K_{a,1} = 6.37$ and p $K_{a,2} = 10.3$ together with a value of $1.8 \cdot 10^{-3}$ mol/L for the total dissolved inorganic carbon (DIC), which results from a correction factor on molal basis of 0.902 for D₂O⁶¹

DIC =
$$c_{\text{CO}_2(\text{aq})} + c_{\text{H},\text{CO}_3} + c_{\text{HCO}_3}^- + c_{\text{CO}_3}^{2-}$$
 (9)

we generate a Bjerrum plot to estimate the amount of ionic species HCO_3^- and CO_3^{2-} at each given sample pH.

Finally, the ionic strength [I] and total concentration of ions c_s present in solution is calculated.

$$c_{\rm s} = c_{\rm NaOH} - c_{\rm -COOH} + c_{\rm HCO_3^-} + c_{\rm CO_3^{2-}}$$
 (10)

Only at pH \gg p $K_{a,2}$ the amount of the carbonate ion CO₃² has to be taken into account, at lower pH the dominant species is the hydrogen carbonate HCO_3^- and for pH \ll p $K_{a,1}$ ions resulting from CO₂ absorption can be neglected (see Figure 11 and Table 6.

ASSOCIATED CONTENT

Supporting Information

The Supporting Information is available free of charge at https://pubs.acs.org/doi/10.1021/acs.macromol.4c00486.

Additional representations of experimental SANS data; partial form factors P(Q); additional experimental structure factors S(Q); rheology data including method, setup and experimental details; photographs of samples (PDF)

AUTHOR INFORMATION

Corresponding Authors

Lutz Willner - Jülich Centre for Neutron Science (JCNS-1), Forschungszentrum Jülich GmbH, 52425 Jülich, Germany; Email: l.willner@fz-juelich.de

Jörg Stellbrink – Jülich Centre for Neutron Science (JCNS-1), Forschungszentrum Jülich GmbH, 52425 Jülich, Germany; orcid.org/0000-0001-6183-3901; Email: j.stellbrink@fzjuelich.de

Lingsam Tea – Jülich Centre for Neutron Science (JCNS-1), Forschungszentrum Jülich GmbH, 52425 Jülich, Germany; Present Address: L.T.: Sorbonne Université, UMR 8234, laboratoire PHENIX, 4, place Jussieu 75005 Paris, France

Luis Willner – Jülich Centre for Neutron Science (JCNS-1), Forschungszentrum Jülich GmbH, 52425 Jülich, Germany

Christin Waldorf – Jülich Centre for Neutron Science (JCNS-1), Forschungszentrum Jülich GmbH, 52425 Jülich, Germany; orcid.org/0009-0002-8917-9299

Olga Matsarskaia – Large Scale Structures Group, Institut Laue-Langevin, 38042 CEDEX 9 Grenoble, France; orcid.org/0000-0002-7293-7287

Ralf Schweins - Large Scale Structures Group, Institut Laue-Langevin, 38042 CEDEX 9 Grenoble, France; o orcid.org/ 0000-0001-8078-2089

Stephan Förster – Jülich Centre for Neutron Science (ICNS-1), Forschungszentrum Jülich GmbH, 52425 Jülich, *Germany*; orcid.org/0000-0002-7323-2449

Complete contact information is available at: https://pubs.acs.org/10.1021/acs.macromol.4c00486

Author Contributions

L.T.: Synthesis and characterization of polymers; SANS, Zeta potential, and rheology experiments and data analysis; manuscript preparation. L.W.: Synthesis and characterization of polymers, preliminary SANS experiments and data analysis. C.W.: Synthesis and characterization of polymers, electrochemical titration experiments and data analysis. O.M.: SANS experiments and data reduction, writing, review. R.S.: SANS experiments and data reduction, writing, review. S.F.: Writing, review, and editing L.W.: Supervision, conceptualization, synthesis and characterization of polymers, manuscript preparation, writing, review, and editing. J.S.: Supervision, conceptualization, SANS experiments and data analysis, manuscript preparation, writing, review, and editing.

Notes

The authors declare no competing financial interest.

ACKNOWLEDGMENTS

We gratefully acknowledge G. Nägele and M. Heinen for helpful discussions and providing the MPB-RMSA software package. We thank K. Kang and J.K.G. Dhont for helpful discussions regarding the CO_2 absorption. Furthermore, we thank R. Biehl for helpful discussions and assistance in the zeta-potential measurements and J. Allgaier for his support in the synthesis and characterisation of the carboxy-terminated polymer. L. Tea acknowledges the Tasso Springer Fellowship program supported by JCNS and Forschunszentrum Jülich GmbH. Finally, we acknowledge ILL for providing SANS beamtime: DOI:10.5291/ILL-DATA.9-11-1995, DOI:10.5291/ILL-DATA.9-10-1629.

REFERENCES

- (1) Stellbrink, J.; Rother, G.; Laurati, M.; Lund, R.; Willner, L.; Richter, D. Poly(ethylene-alt-propylene)—poly(ethylene oxide) diblock copolymer micelles: a colloidal model system with tunable softness. *J. Phys.: Condens. Matter* **2004**, *16*, S3821—S3834.
- (2) Vlassopoulos, D.; Cloitre, M. Tunable rheology of dense soft deformable colloids. *Curr. Opin. Colloid Interface Sci.* **2014**, 19, 561–574
- (3) Likos, C. N.; Löwen, H.; Watzlawek, M.; Abbas, B.; Jucknischke, O.; Allgaier, J.; Richter, D. Star Polymers Viewed as Ultrasoft Colloidal Particles. *Phys. Rev. Lett.* **1998**, *80*, 4450–4453.
- (4) Zinn, T.; Willner, L.; Lund, R.; Pipich, V.; Appavou, M. S.; Richter, D. Surfactant or block copolymer micelles? Structural properties of a series of well-defined n-alkyl-PEO micelles in water studied by SANS. *Soft Matter* **2014**, *10*, 5212–20.
- (5) Laflèche, F.; Nicolai, T.; Durand, D.; Gnanou, Y.; Taton, D. Association of Adhesive Spheres Formed by Hydrophobically End-Capped PEO. 2. Influence of the Alkyl End-Group Length and the Chain Backbone Architecture. *Macromolecules* **2003**, *36*, 1341–1348.
- (6) Renou, F.; Nicolai, T.; Nicol, E.; Benyahia, L. Structure and Viscoelasticity of Mixed Micelles Formed by Poly(ethylene oxide) End Capped with Alkyl Groups of Different Length. *Langmuir* 2009, 25, 515–521.
- (7) Gupta, S.; Camargo, M.; Stellbrink, J.; Allgaier, J.; Radulescu, A.; Lindner, P.; Zaccarelli, E.; Likos, C. N.; Richter, D. Dynamic phase diagram of soft nanocolloids. *Nanoscale* **2015**, *7*, 13924–13934.
- (8) Lund, R.; Willner, L.; Stellbrink, J.; Radulescu, A.; Richter, D. Role of Interfacial Tension for the Structure of PEP-PEO Polymeric Micelles. A Combined SANS and Pendant Drop Tensiometry Investigation. *Macromolecules* **2004**, *37*, 9984–9993.
- (9) Laurati, M.; Stellbrink, J.; Lund, R.; Willner, L.; Richter, D.; Zaccarelli, E. Starlike Micelles with Starlike Interactions: A Quantitative Evaluation of Structure Factors and Phase Diagram. *Phys. Rev. Lett.* **2005**, *94*, 195504.
- (10) Laurati, M.; Stellbrink, J.; Lund, R.; Willner, L.; Zaccarelli, E.; Richter, D. Asymmetric poly(ethylene-alt-propylene)-poly(ethylene oxide) micelles: A system with starlike morphology and interactions. *Phys. Rev. E* **2007**, *76*, 041503.
- (11) Gupta, S.; Stellbrink, J.; Zaccarelli, E.; Likos, C. N.; Camargo, M.; Holmqvist, P.; Allgaier, J.; Willner, L.; Richter, D. Validity of the Stokes-Einstein Relation in Soft Colloids up to the Glass Transition. *Phys. Rev. Lett.* **2015**, *115*, 128302.
- (12) Sefcik, J.; Verduyn, M.; Storti, G.; Morbidelli, M. Charging of Latex Particles Stabilized by Sulfate Surfactant. *Langmuir* **2003**, *19*, 4778–4783.
- (13) Smith, G. N.; Hallett, J. E.; Eastoe, J. Celebrating Soft Matter's 10th Anniversary: Influencing the charge of poly(methyl methacrylate) latexes in nonpolar solvents. *Soft Matter* **2015**, *11*, 8029–8041.

- (14) Yethiraj, A.; van Blaaderen, A. A colloidal model system with an interaction tunable from hard sphere to soft and dipolar. *Nature* **2003**, 421. 513–517.
- (15) Nisato, G.; Ivkov, R.; Amis, E. J. Structure of Charged Dendrimer Solutions As Seen by Small-Angle Neutron Scattering. *Macromolecules* **1999**, *32*, 5895–5900.
- (16) Nisato, G.; Ivkov, R.; Amis, E. J. Size Invariance of Polyelectrolyte Dendrimers. *Macromolecules* **2000**, 33, 4172–4176.
- (17) Huang, Q. R.; Dubin, P. L.; Moorefield, C. N.; Newkome, G. R. Counterion Binding on Charged Spheres: Effect of pH and Ionic Strength on the Mobility of Carboxyl-Terminated Dendrimers. *J. Phys. Chem. B* **2000**, *104*, 898–904.
- (18) Liu, Y.; Chen, C.-Y.; Chen, H.-L.; Hong, K.; Shew, C.-Y.; Li, X.; Liu, L.; Melnichenko, Y. B.; Smith, G. S.; Herwig, K. W.; Porcar, L.; Chen, W.-R. Electrostatic Swelling and Conformational Variation Observed in High-Generation Polyelectrolyte Dendrimers. *J. Phys. Chem. Lett.* **2010**, *1*, 2020–2024.
- (19) Porcar, L.; Liu, Y.; Verduzco, R.; Hong, K.; Butler, P. D.; Magid, L. J.; Smith, G. S.; Chen, W.-R. Structural Investigation of PAMAM Dendrimers in Aqueous Solutions Using Small-Angle Neutron Scattering: Effect of Generation. *J. Phys. Chem. B* **2008**, *112*, 14772–14778.
- (20) Porcar, L.; Hong, K.; Butler, P. D.; Herwig, K. W.; Smith, G. S.; Liu, Y.; Chen, W.-R. Intramolecular Structural Change of PAMAM Dendrimers in Aqueous Solutions Revealed by Small-Angle Neutron Scattering. *J. Phys. Chem. B* **2010**, *114*, 1751–1756.
- (21) Förster, S.; Abetz, V.; Müller, A. H. E. *Polyelectrolytes with Defined Molecular Architecture II*; Springer: Berlin, Heidelberg, 2004; pp 173–210. DOI: 10.1007/b11351.
- (22) Förster, S.; Hermsdorf, N.; Böttcher, C.; Lindner, P. Structure of Polyelectrolyte Block Copolymer Micelles. *Macromolecules* **2002**, 35, 4096–4105.
- (23) Lee, A. S.; Bütün, V.; Vamvakaki, M.; Armes, S. P.; Pople, J. A.; Gast, A. P. Structure of pH-Dependent Block Copolymer Micelles: Charge and Ionic Strength Dependence. *Macromolecules* **2002**, *35*, 8540–8551.
- (24) Sprouse, D.; Jiang, Y.; Laaser, J. E.; Lodge, T. P.; Reineke, T. M. Tuning Cationic Block Copolymer Micelle Size by pH and Ionic Strength. *Biomacromolecules* **2016**, *17*, 2849–2859.
- (25) Papagiannopoulos, A.; Karayianni, M.; Mountrichas, G.; Pispas, S.; Radulescu, A. Self-Assembled Nanoparticles from a Block Polyelectrolyte in Aqueous Media: Structural Characterization by SANS. J. Phys. Chem. B 2010, 114, 7482–7488.
- (26) Plamper, F.; Xu, Y.; Yuan, J.; Ballauff, M.; Müller, A. H. E. New Smart Materials via Metal Mediated Macromolecular Engineering; Springer Netherlands, 2009; pp 17–36. DOI: 10.1007/978-90-481-3278-2 2.
- (27) Boué, F.; Combet, J.; Demé, B.; Heinrich, M.; Zilliox, J.-G.; Rawiso, M. SANS from Salt-Free Aqueous Solutions of Hydrophilic and Highly Charged Star-Branched Polyelectrolytes. *Polymers* **2016**, *8*, 228.
- (28) Jusufi, A.; Likos, C. N.; Löwen, H. Conformations and Interactions of Star-Branched Polyelectrolytes. *Phys. Rev. Lett.* **2001**, 88, 018301.
- (29) Chremos, A.; Douglas, J. F. Solution properties of star polyelectrolytes having a moderate number of arms. *J. Chem. Phys.* **2017**, *147*, 044906.
- (30) Zhou, B.; Gasser, U.; Fernandez-Nieves, A. Measuring the counterion cloud of soft microgels using SANS with contrast variation. *Nat. Commun.* **2023**, *14*, 1–7.
- (31) Heinen, M.; Holmqvist, P.; Banchio, A. J.; Nägele, G. Pair structure of the hard-sphere Yukawa fluid: An improved analytic method versus simulations, Rogers-Young scheme, and experiment. *J. Chem. Phys.* **2011**, *134*, 044532.
- (32) Zinn, T.; Willner, L.; Lund, R. Nanoscopic confinement through self-assembly: crystallization within micellar cores exhibits simple Gibbs-Thomson behavior. *Phys. Rev. Lett.* **2014**, *113*, 238305.

- (33) Amann, M.; Willner, L.; Stellbrink, J.; Radulescu, A.; Richter, D. Studying the concentration dependence of the aggregation number of a micellar model system by SANS. *Soft Matter* **2015**, *11*, 4208–4217.
- (34) König, N.; Willner, L.; Pipich, V.; Zinn, T.; Lund, R. Cooperativity during Melting and Molecular Exchange in Micelles with Crystalline Cores. *Phys. Rev. Lett.* **2019**, *122*, 078001.
- (35) König, N.; Willner, L.; Lund, R. Structure and thermodynamics of mixed polymeric micelles with crystalline cores: tuning properties via co-assembly. *Soft Matter* **2019**, *15*, 7777–7786.
- (36) König, N.; Willner, L.; Carlström, G.; Zinn, T.; Knudsen, K. D.; Rise, F.; Topgaard, D.; Lund, R. Spherical Micelles with Nonspherical Cores: Effect of Chain Packing on the Micellar Shape. *Macromolecules* **2020**, *53*, 10686–10698.
- (37) Zinn, T.; Willner, L.; Pipich, V.; Richter, D.; Lund, R. Effect of Core Crystallization and Conformational Entropy on the Molecular Exchange Kinetics of Polymeric Micelles. *ACS Macro Lett.* **2015**, *4*, 651–655.
- (38) Lodge, T. P.; Seitzinger, C. L.; Seeger, S. C.; Yang, S.; Gupta, S.; Dorfman, K. D. Dynamics and Equilibration Mechanisms in Block Copolymer Particles. *ACS Polymers Au* **2022**, *2*, 397–416.
- (39) Chiappisi, L. Polyoxyethylene alkyl ether carboxylic acids: An overview of a neglected class of surfactants with multiresponsive properties. *Adv. Colloid Interface Sci.* **2017**, 250, 79–94.
- (40) Crivello, C.; Lazzara, G.; Chiappisi, L. On the effect of the nature of counterions on the self-assembly of polyoxyethylene alkyl ether carboxylic acids. *Soft Matter* **2020**, *16*, 7137–7143.
- (41) Hayward, D. W.; Chiappisi, L.; Prévost, S.; Schweins, R.; Gradzielski, M. A Small-Angle Neutron Scattering Environment for In-Situ Observation of Chemical Processes. *Sci. Rep.* **2018**, *8*, 1–11.
- (42) Hayward, D. W.; Chiappisi, L.; Teo, J. H.; Prévost, S.; Schweins, R.; Gradzielski, M. Neutralisation rate controls the self-assembly of pH-sensitive surfactants. *Soft Matter* **2019**, *15*, 8611–8620.
- (43) Verwey, E. J. W.; Overbeek, J. T. G. Theory of the stability of lyophobic colloids; Elsevier Pub. Co. Inc.: New York, Amsterdam, London, Brussels, 1948.
- (44) Hansen, J.-P.; Hayter, J. B. A rescaled MSA structure factor for dilute charged colloidal dispersions. *Mol. Phys.* **1982**, *46*, 651–656.
- (45) Snook, I. K.; Hayter, J. B. Static structure of strongly interacting colloidal particles. *Langmuir* **1992**, *8*, 2880–2884.
- (46) Qiu, J. C.; Pradhan, P. P.; Blanck, N. B.; Bobbitt, J. M.; Bailey, W. F. Selective Oxoammonium Salt Oxidations of Alcohols to Aldehydes and Aldehydes to Carboxylic Acids. *Org. Lett.* **2012**, *14*, 350–353.
- (47) Mercadante, M. A.; Kelly, C. B.; Bobbitt, J. M.; Tilley, L. J.; Leadbeater, N. E. Synthesis of 4-acetamido-2,2,6,6-tetramethylpiperidine-1-oxoammonium tetrafluoroborate and 4-acetamido-(2,2,6,6-tetramethyl-piperidin-1-yl)oxyl and their use in oxidative reactions. *Nat. Protoc.* **2013**, *8*, 666–676.
- (48) van Gruijthuijsen, K.; Obiols-Rabasa, M.; Heinen, M.; Nägele, G.; Stradner, A. Sterically Stabilized Colloids with Tunable Repulsions. *Langmuir* **2013**, *29*, 11199–11207.
- (49) Daoud, M.; Cotton, J. P. Star shaped polymers: a model for the conformation and its concentration dependence. *J. Phys.* (*Paris*) **1982**, 43, 531–538.
- (50) Halperin, A. Polymeric Micelles a Star Model. *Macromolecules* 1987, 20, 2943–2946.
- (51) Pipich, V. QtiSAS: user-friendly program for reduction, visualization, analysis and fit of SA(N)S data, URL https://www.qtisas.com. 2020,.
- (52) Sommer, C.; Pedersen, J. S.; Stein, P. C. Apparent Specific Volume Measurements of Poly(ethylene oxide), Poly(butylene oxide), Poly(propylene oxide), and Octadecyl Chains in the Micellar State as a Function of Temperature. *J. Phys. Chem. B* **2004**, *108*, 6242–6249.
- (53) Wu, C.; Chan, D. Y.; Tabor, R. F. A simple and accurate method for calculation of the structure factor of interacting charged spheres. *J. Colloid Interface Sci.* **2014**, 426, 80–82.

- (54) Hayter, J. B.; Penfold, J. An analytic structure factor for macroion solutions. *Mol. Phys.* **1981**, 42, 109–118.
- (55) Chang, M.-C.; Tung, C.-H.; Chang, S.-Y.; Carrillo, J. M.; Wang, Y.; Sumpter, B. G.; Huang, G.-R.; Do, C.; Chen, W.-R. A machine learning inversion scheme for determining interaction from scattering. *Communications Physics* **2022**, *5*, 1–8.
- (56) Hansen, J.-P.; Verlet, L. Phase Transitions of the Lennard-Jones System. *Phys. Rev.* **1969**, *184*, 151–161.
- (57) Puaud, F.; Nicolai, T.; Nicol, E.; Benyahia, L.; Brotons, G. Dynamic Arm Exchange Facilitates Crystallization and Jamming of Starlike Polymers by Spontaneous Fine-Tuning of the Number of Arms. *Phys. Rev. Lett.* **2013**, *110*, 028302.
- (58) Kremer, K.; Robbins, M. O.; Grest, G. S. Phase Diagram of Yukawa Systems: Model for Charge-Stabilized Colloids. *Phys. Rev. Lett.* **1986**, *57*, 2694–2697.
- (59) Kang, K.; Wilk, A.; Patkowski, A.; Dhont, J. K. G. Diffusion of spheres in isotropic and nematic networks of rods: Electrostatic interactions and hydrodynamic screening. *J. Chem. Phys.* **2007**, *126*, 214501.
- (60) Zeebe, R. E., Wolf-Gladrow, D. A., Eds. CO2 in seawater; Elsevier oceanography series 0422–9894 65; Elsevier: Amsterdam, 2010; Master and use copy. Digital master created according to Benchmark for Faithful Digital Reproductions of Monographs and Serials, Version 1. Digital Library Federation, December 2002.
- (61) Curry, J.; Hazelton, C. L. The Solubility of Carbon Dioxide in Deuterium Oxide at 25°1. *J. Am. Chem. Soc.* **1938**, *60*, 2771–2773.